
SINGLE-SNAPSHOT MACHINE LEARNING FOR TURBULENCE SUPER RESOLUTION

A PREPRINT

Kai Fukami* and Kunihiko Taira

Department of Mechanical and Aerospace Engineering
University of California, Los Angeles, CA 90095, USA

*Corresponding author: kfukami1@g.ucla.edu

September 10, 2024

ABSTRACT

Modern machine-learning techniques are generally considered data-hungry. However, this may not be the case for turbulence as each of its snapshots can hold more information than a single data file in general machine-learning applications. This study asks the question of whether nonlinear machine-learning techniques can effectively extract physical insights even from as little as a *single* snapshot of a turbulent vortical flow. As an example, we consider machine-learning-based super-resolution analysis that reconstructs a high-resolution field from low-resolution data for two-dimensional decaying turbulence. We reveal that a carefully designed machine-learning model trained with flow tiles sampled from only a single snapshot can reconstruct vortical structures across a range of Reynolds numbers. Successful flow reconstruction indicates that nonlinear machine-learning techniques can leverage scale-invariance properties to learn turbulent flows. We further show that training data of turbulent flows can be cleverly collected from a single snapshot by considering characteristics of rotation and shear tensors. The present findings suggest that embedding prior knowledge in designing a model and collecting data is important for a range of data-driven analyses for turbulent flows. More broadly, this work hopes to stop machine-learning practitioners from being wasteful with turbulent flow data.

1 Introduction

By gazing at a turbulent flow acquired from numerical simulation or experiment, we can admire the rich physics that involves swirling, stretching, and diffusion. Turbulence also presents multi-scale characteristics over broad length scales [1]. In high Reynolds number turbulent flows, the rich phenomena and characteristics are exhibited at any instance in time. We argue that even a single snapshot of turbulent flow can hold sufficient information to train machine-learning models. This paper poses a question of whether a commonly used big data set is required for training machine-learning models in studying turbulence.

There have been increased usages of modern machine-learning techniques to analyze, model, estimate, and control turbulent flows [2]. These applications include subgrid-scale modeling [3], reduced-order modeling [4], super resolution/flow reconstruction [5, 6], and flow control [7, 8]. These machine-learning models require enormous amount of training data, which is generally significantly larger than those necessitated by traditional analysis techniques.

However, it may be possible to extract important vortical features without such large data sets since even a single turbulent flow snapshot contains multi-scale, scale-invariant structures. To achieve meaningful learning from a single snapshot, we consider training machine-learning models through subsampling and leveraging turbulent statistics. We further note that it is important that machine-learning models have appropriate architectures and learning formulation that fold in physics [9, 10, 11, 12].

This study considers data-driven analysis using only a single training snapshot of turbulent flow. As an example, we perform machine-learning-based super-resolution analysis for two-dimensional decaying turbulence. We show that flow reconstruction over a range of Reynolds numbers is possible with nonlinear machine learning by cleverly sampling data

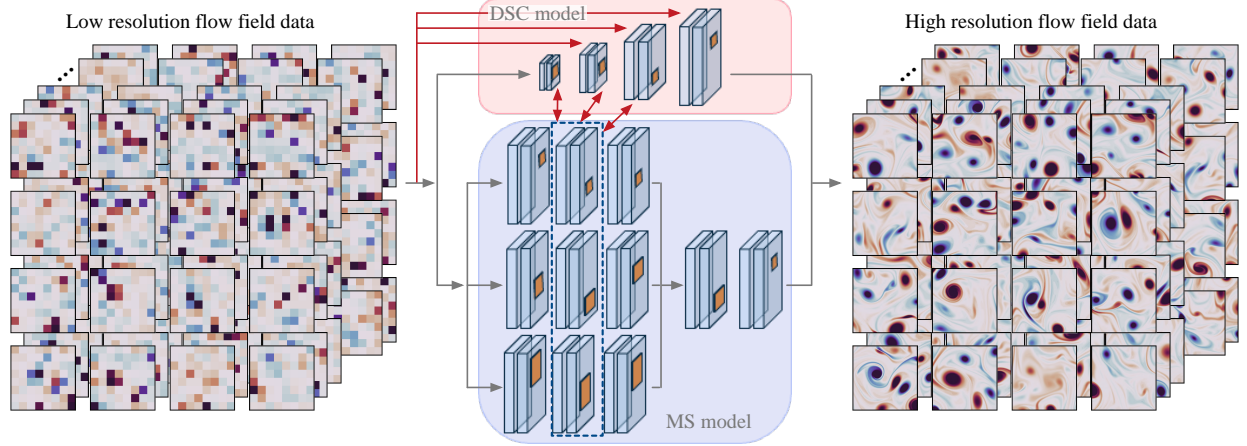


Figure 1: Interconnected DSC/MS model [12] for super-resolution reconstruction of two-dimensional decaying turbulence.

from a single snapshot. The present results show that a large data set is not necessarily needed for machine learning of turbulent flows.

This paper is organized as follows. The approach is described in section 2. Results from the single-snapshot super-resolution analysis are presented in section 3. Conclusions are offered in section 4.

2 Approach

The objective of this study is to show that it is possible to perform data-driven analysis of turbulent flows with a very limited amount of training data – even from a single snapshot. For the present analysis, we consider machine-learning-based super-resolution reconstruction of vortical flows [13]. A machine-learning model \mathcal{F} is trained to reconstruct a high-resolution flow field \mathbf{q}_{HR} from a low-resolution data \mathbf{q}_{LR} :

$$\mathbf{q}_{\text{HR}} = \mathcal{F}(\mathbf{q}_{\text{LR}}; \mathbf{w}), \quad (1)$$

where \mathbf{w} denotes the weights inside the model. We use the vorticity field ω as a data attribute. In this study, the model \mathcal{F} is trained with a collection of subdomains sampled from only *a single snapshot* of two-dimensional isotropic turbulence. The model is then tested with independent snapshots. If the model \mathcal{F} successfully learns the relationship between low- and high-resolution vortical flows from a single training snapshot, we expect that the reconstruction would be possible even for independent testing conditions.

For machine-learning-based super resolution of turbulent flows, the model \mathcal{F} needs to be carefully designed to accommodate a range of length scales while accounting for rotational and translational invariance of vortical structures [5]. This study uses the interconnected hybrid downsampled skip-connection/multi-scale (DSC/MS) model [12] based on convolutional neural networks (CNN) [14], as illustrated in figure 1. Between the layers $(l-1)$ and (l) , the CNN learns the nonlinear relationship between input and output data by extracting spatial features of given data through filtering operations,

$$c_{ij_n}^{(l)} = \varphi \left(\sum_{m=1}^M \sum_{p=0}^{H-1} \sum_{q=0}^{H-1} h_{pqmn}^{(l)} c_{i+p-G, j+q-G, m}^{(l-1)} + b_n^{(l)} \right), \quad (2)$$

where $G = \lfloor H/2 \rfloor$, H is the width and height of the filter h , M is the number of input channel, n is the number of output channel, b is the bias, and φ is the activation function. By using a nonlinear function for φ , the convolutional networks can account for nonlinearities in learning features from training data.

The DSC model (boxed in red) includes up/downsampling operations and skip connections, capturing rotational and translational invariance [15]. The MS model (boxed in blue) consists of three different sizes of filter operations, enabling the model to learn a range of length scales in turbulent flows. Furthermore, these two networks are internally connected via skip connections [16] to enhance the correlation of the intermediate input and output from both subnetworks in the training process. We refer to Fukami et al. [12] and a sample code (<http://www.seas.ucla.edu/fluidflow/codes.html>) for further details on the present machine-learning model. In this study, model \mathcal{F} is trained such that

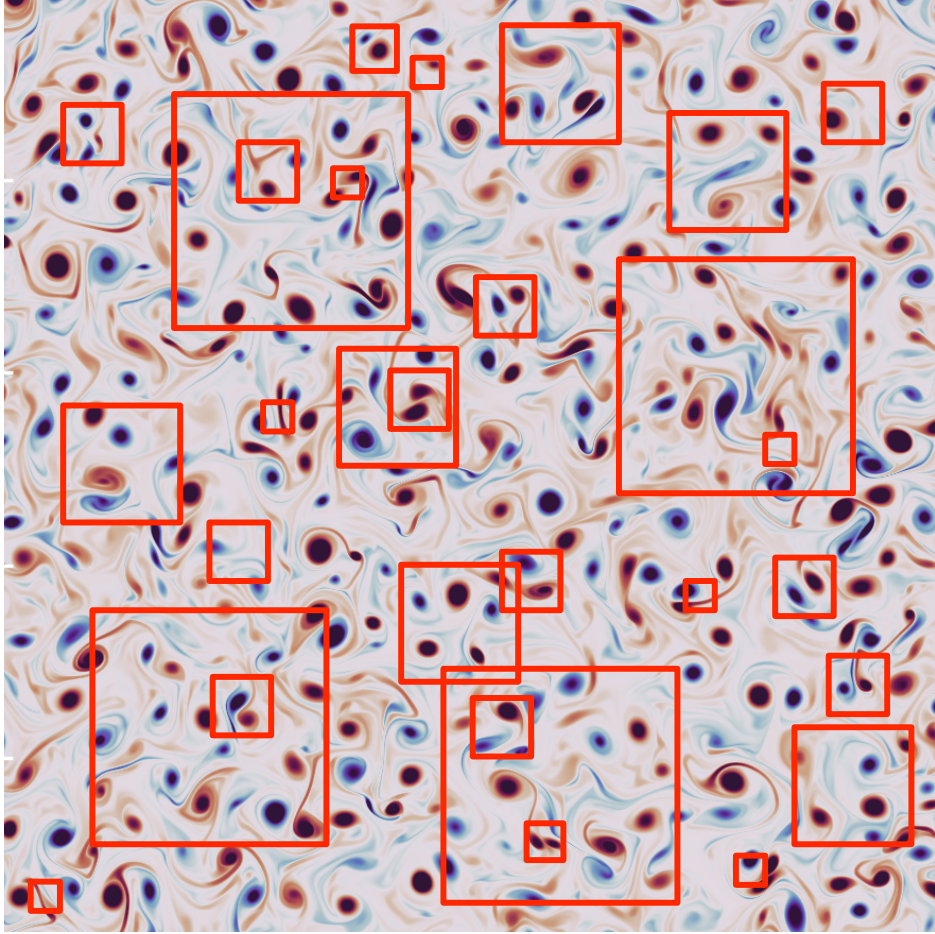


Figure 2: Two-dimensional isotropic vorticity field. Red boxes are example flow tiles used for training.

weights \mathbf{w} are optimized through

$$\mathbf{w}^* = \operatorname{argmin}_{\mathbf{w}} \|\omega_{\text{HR}} - \mathcal{F}(\omega_{\text{LR}}; \mathbf{w})\|_2, \quad (3)$$

where ω_{HR} and ω_{LR} represent the reference high and the low-resolution input vorticity fields, respectively.

Two-dimensional decaying isotropic turbulence is considered in the present study. The flow field data are generated with direct numerical simulation [17] that numerically solves the two-dimensional vorticity transport equation

$$\frac{\partial \omega}{\partial t} + \mathbf{u} \cdot \nabla \omega = \frac{1}{Re_0} \nabla^2 \omega, \quad (4)$$

where $\mathbf{u} = (u, v)$ represents the velocity field and $Re_0 = u^* l_0^* / \nu$ is the initial Reynolds number. Here, u^* is the characteristic velocity defined as the square root of the spatially averaged initial kinetic energy, $l_0^* = [2\overline{u^2}(t_0)/\overline{\omega^2}(t_0)]^{1/2}$ is the initial integral length, and ν is the kinematic viscosity. The overline denotes the spatial average. The computational domain is a bi-periodic square with length $L = 1$.

The baseline super-resolution analysis is performed with the model trained with a single snapshot shown in figure 2 with $Re_0 = 1580$. Various vortical structures, including counter-rotating and co-rotating vortices and shear layers, of different length scales are contained in this single snapshot. The number of computational grid points N^2 is set to 1024^2 , satisfying $k_{\text{max}} \eta \geq 1$, where k_{max} is the maximum wavenumber and η is the Kolmogorov length scale, to ensure that the DNS resolves all flow scales. The simulation for training data preparation is initialized with a distribution composed of randomly-placed Taylor vortices [18] with random strengths and sizes. The snapshot is collected after the flow reaches the decaying regime.

The present training data is comprised of square-sized subdomain samples randomly collected from the single snapshot with four different sizes of $L_{\text{sub}} = \{0.03125, 0.0625, 0.125, 0.25\}$, as illustrated in figure 2. The subdomain data are

then resized to be $N_{\text{ML}}^2 = 128^2$ for the present data-driven analysis. The dependence of super-resolution reconstruction on the choice of a single snapshot is examined later.

Test snapshots in this study are prepared from three different simulations. The initial Reynolds numbers and the number of grid points are, respectively, $Re_0 = \{80.4, 177, 442\}$ and $N = \{128, 256, 512\}$, satisfying $k_{\text{max}}\eta \geq 1$. These settings are intended to generate test snapshots that include a similar size of vortical structures to that in the subdomains of the single snapshot. Once the test snapshots are collected from the simulations, they are resized to be $N_{\text{ML}} = 128$. The present machine-learning model \mathcal{F} reconstructs the high-resolution vorticity flow field of size 128^2 from the corresponding low-resolution data of size 8^2 generated by average pooling [13]. The input and output data are normalized by the instantaneous maximum value of absolute vorticity, $\max(|\omega|)$ to account for the magnitude difference of vorticity fields across the Reynolds number.

3 Results

We apply the super-resolution model trained with a single snapshot to decaying turbulence at three different test Re . The reconstruction by the DSC/MS model is compared to bicubic interpolation, as shown in figure 3. Let us first use 2,000 local tiles in total for training the baseline model. The value listed underneath each figure reports the L_2 error norm $\epsilon = \|\omega_{\text{HR}} - \mathcal{F}(\omega_{\text{LR}})\|_2 / \|\omega_{\text{HR}}\|_2$. As the bicubic interpolation simply smooths the given low-resolution data, the reconstructed fields do not provide any fine-scale information, resulting in a high L_2 error.

To improve the reconstruction of fine-scale structures, let us consider the DSC/MS model-based super resolution. The reconstructed fields by the DSC/MS model show improved agreement with the reference data. In addition to large-scale structures, rotational and shear-layer structures are also well represented compared to bicubic interpolation, reporting only 10-20% L_2 error across the range of Reynolds numbers. Note that this level of error suggests accurate reconstruction that captures turbulent coherent structures since the spatial L_2 norm is a strict comparative measure [19].

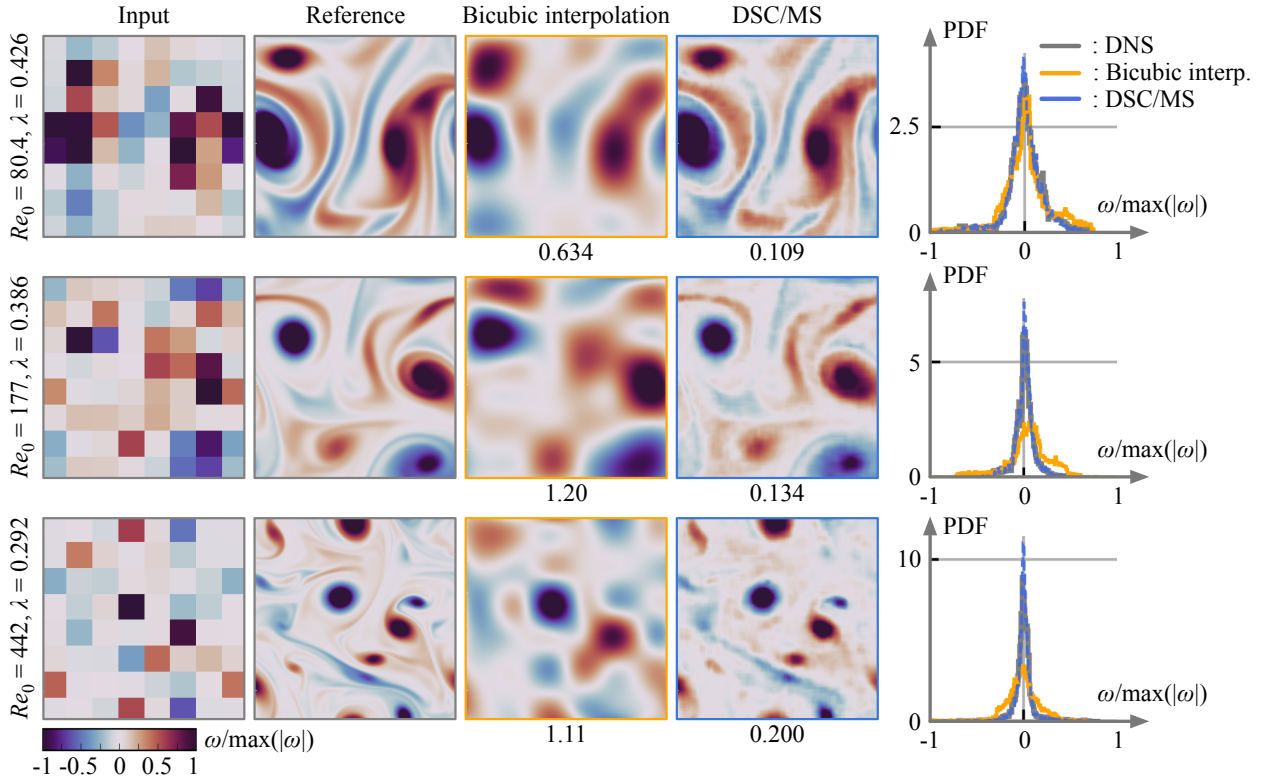


Figure 3: A single snapshot super-resolution of two-dimensional decaying turbulence. Its accuracy is assessed with test snapshots from three different simulations. The instantaneous Taylor length scale $\lambda(t)$ for a representative test snapshot is reported along with each Re_0 . The value underneath each contour is the L_2 error norm. The probability density function (PDF) for test snapshots at each Reynolds number is also shown.

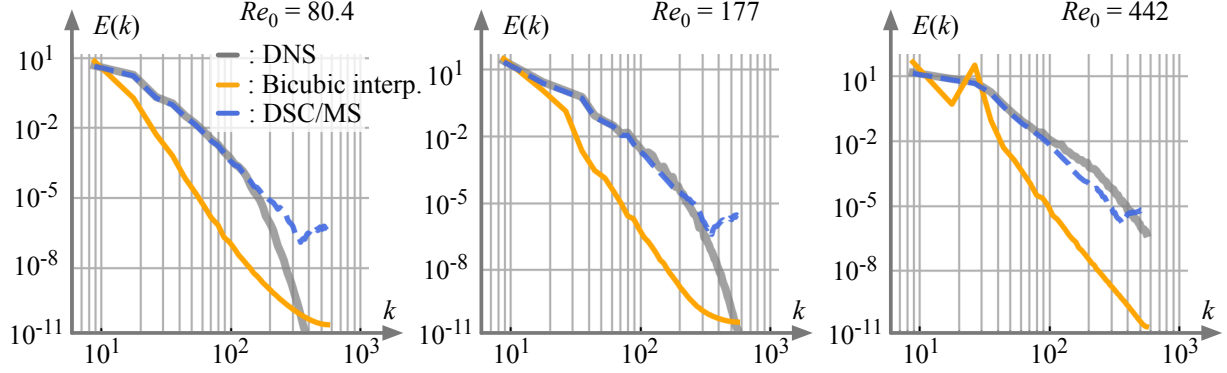


Figure 4: Kinetic energy spectrum $E(k)$ of the reconstructed vorticity fields.

The reconstruction performance is also examined with the probability density function (PDF) of the vorticity field, as presented in figure 3. For the case of $Re_0 = 80.4$, the curves obtained from both the bicubic interpolation and the DSC/MS model are in agreement with the reference data. However, the curve for the bicubic interpolation (colored in orange) deviates for the tail of the distribution, implying the failure in reconstructing strong rotation structures with low probability.

As the test Re increases, the bicubic interpolation starts struggling to reconstruct the vorticity across its distribution. This is because the smallest and largest scales spread wider by increasing the test Reynolds number. In contrast, the distributions obtained by the present DSC/MS model are almost indistinguishable compared to those with the reference DNS, supporting statistically accurate reconstruction. These results imply that even just a single turbulent flow snapshot contains a variety of vortical structures across different length scales, which can be extracted by the present machine-learning approach.

To further examine the reconstruction performance across spatial length scales, let us present in figure 4 the kinetic energy spectrum $E(k)$, where k is the wavenumber. While the bicubic interpolation significantly underestimates the energy across the wavenumbers, the machine-learning model provides reasonable agreement up to $k \approx 200$ for $Re_0 = 80.4$ and 177 and $k \approx 100$ for $Re_0 = 442$. The difference in the high-wavenumber regime is due to the low correlation between the low- and high-wavenumber components, which is often observed in supervised learning-based super-resolution of turbulent flows [12]. A remedy for improved matching over the high wavenumber could be attained by using algorithms such as generative learning [20, 21]. The results here indicate that the current model can learn the energy distribution over the spatial length scales and Reynolds numbers from only a single snapshot.

The successful reconstruction above is supported by the richness of vortical information contained in the training snapshot depicted in figure 2. In other words, the single snapshot to be used for training must be rich with information. To examine this point, we further consider 150 different flow fields generated by 20 different initial conditions with $N \in [128, 2048]$ and $Re_0 \in [40, 2050]$. We perform the single-snapshot training with these snapshots covering a variety of flow realizations regarding the size and shape of vortices, as shown in figure 5.

To quantify the effect of the single-snapshot choice in training on the reconstruction performance for test data, we use the ratio of the Taylor length scale between training and test snapshots, $\lambda_{\text{test}}/\lambda_{\text{single}}$, where λ represents the Taylor length scale and subscripts “test” and “single” denote test and training (single) snapshots, respectively. The relationship between this ratio and the reconstruction error across the different numbers of local tiles n_s generated from a vorticity snapshot is presented in figure 6(a). For each case, a 3-fold cross-validation is performed and the averaged error is reported. The reconstruction improves for large $\lambda_{\text{test}}/\lambda_{\text{single}}$. In other words, large λ_{test} (low test Re snapshots) or small λ_{single} (high training Re snapshots) provides low reconstruction error.

The error decreases by increasing the number of local tiles n_s across the length-scale ratio. While this error reduction for large n_s is expected, it is worth pointing out that lower n_s is needed as the ratio $\lambda_{\text{test}}/\lambda_{\text{single}}$ increases to achieve the same level of reconstruction. In other words, quantitative reconstruction can be achieved with a smaller number of local tiles in the single-snapshot training with a small λ_{single} that generally corresponds to a high- Re field including many vortical structures. These observations imply that in addition to the number of local samples or snapshots, the amount of information contained in the training data should also be considered when analyzing turbulent flows.

Let us focus on the baseline case of $\lambda_{\text{single}} = 0.0425$, depicted in figure 2, to further discuss the effect of the number of local tiles n_s across the test Reynolds number, as shown in figure 6(b). The averaged error over cross-validation is

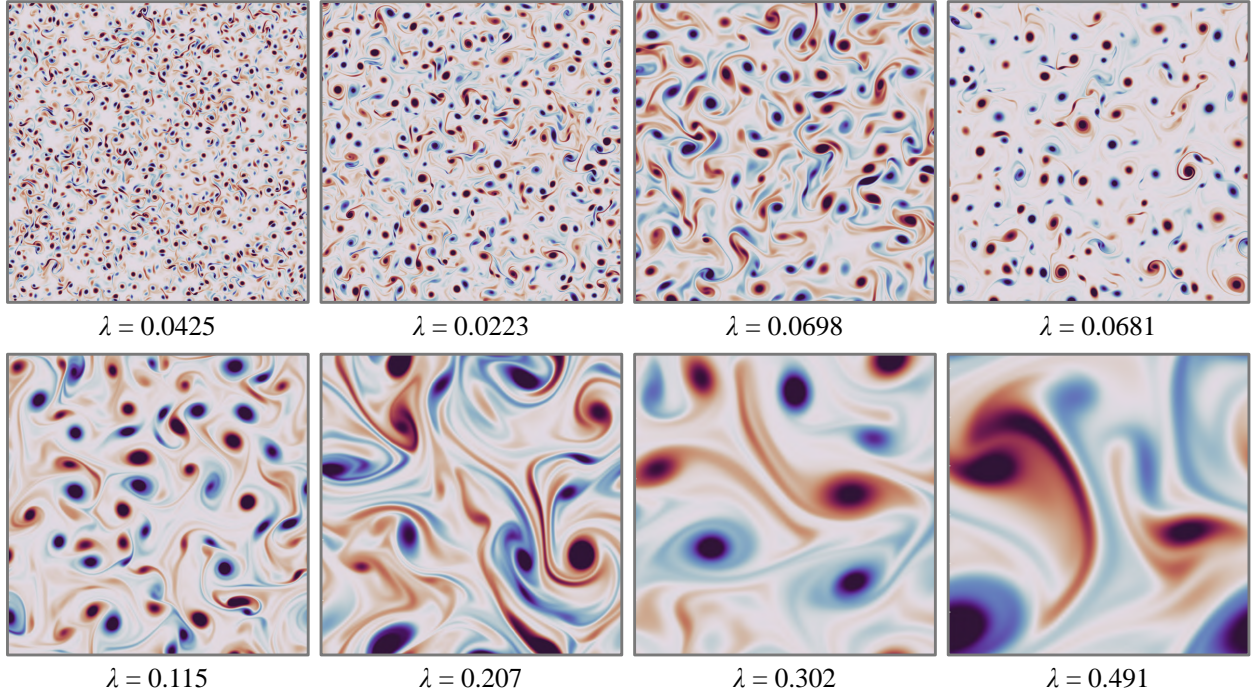


Figure 5: Example snapshots used for single-snapshot training. The value underneath each snapshot is the instantaneous Taylor length scale $\lambda(t)$.

reported while the maximum and minimum errors at each n_s are shown with shading. Across n_s , the reconstruction error at a higher Re is larger compared to lower Re flows, likely because of larger differences in the vortical length scales appearing in the flow. As n_s increases, the reconstruction performance is improved across the Reynolds number. Notably, the present model achieves qualitative reconstruction for large-scale structures even with merely 250 training samples, as presented in figure 6(c). Even in such a modest number of local tiles, there exist physical insights (relations) that can be extracted by the present super-resolution model.

Once n_s exceeds 2,000, the error curves across the Reynolds number plateau, implying that extracted data of vortical flows becomes redundant from the perspective of learning. While the above model is trained with randomly sampled local tiles from a single snapshot, the present nonlinear machine-learning model can achieve quantitative reconstruction even with a much smaller number of local subdomains by sampling them in a smart manner based on some knowledge of the vortical flows.

The idea here is to avoid sampling local tiles that are not informative. To preferentially sample informative local subdomains that include insightful rotational motions and shear layers, we consider the moments of rotation and strain tensors, W and D . The two-dimensional probability density functions based on the mean (first moment), standard deviation (second moment, σ), skewness (third moment, S), and flatness (fourth moment, F) of W and D with $L_{\text{sub}} = 0.0625$ are presented in figure 7(a). The 97% confidence interval is also depicted on each PDF map. Compared to the first and second moment-based PDFs, the third and fourth moment-based PDFs provide a sharper distribution of snapshots, as observed from the difference in the size of 97% confidence interval area. Furthermore, we observe that local tiles containing various structures such as flow fields (i) and (ii) appear in the region with high probability while less informative tiles such as flow fields (iii) and (iv) are seen in the area with lower probability when using the skewness.

Based on the findings above, data sampling informed by the moment probability for single-snapshot training with $n_s = 250$ is performed, as shown in figure 7(b). For comparison, the first and second moment-based sampling are also considered. While the lower-order moment-based training presents similar reconstruction performance to the case in which the location of subdomains is randomly determined, the third and fourth moment-based sampling models provide enhanced reconstruction with the same number of local tiles, revealing vortices and shear-layer structures with finer details. Note that the error level of the higher-order moment-based sampling with $n_s = 250$ becomes the same as that of random sampling with $n_s = 2000$, achieving significant reduction in the required number of training subsamples for

accurate reconstruction. These observations suggest that machine-learning-based analyses traditionally recognized as expensive, data-hungry approaches can take advantage of the scale-invariant property in analyzing turbulent vortical flows from much smaller data sets.

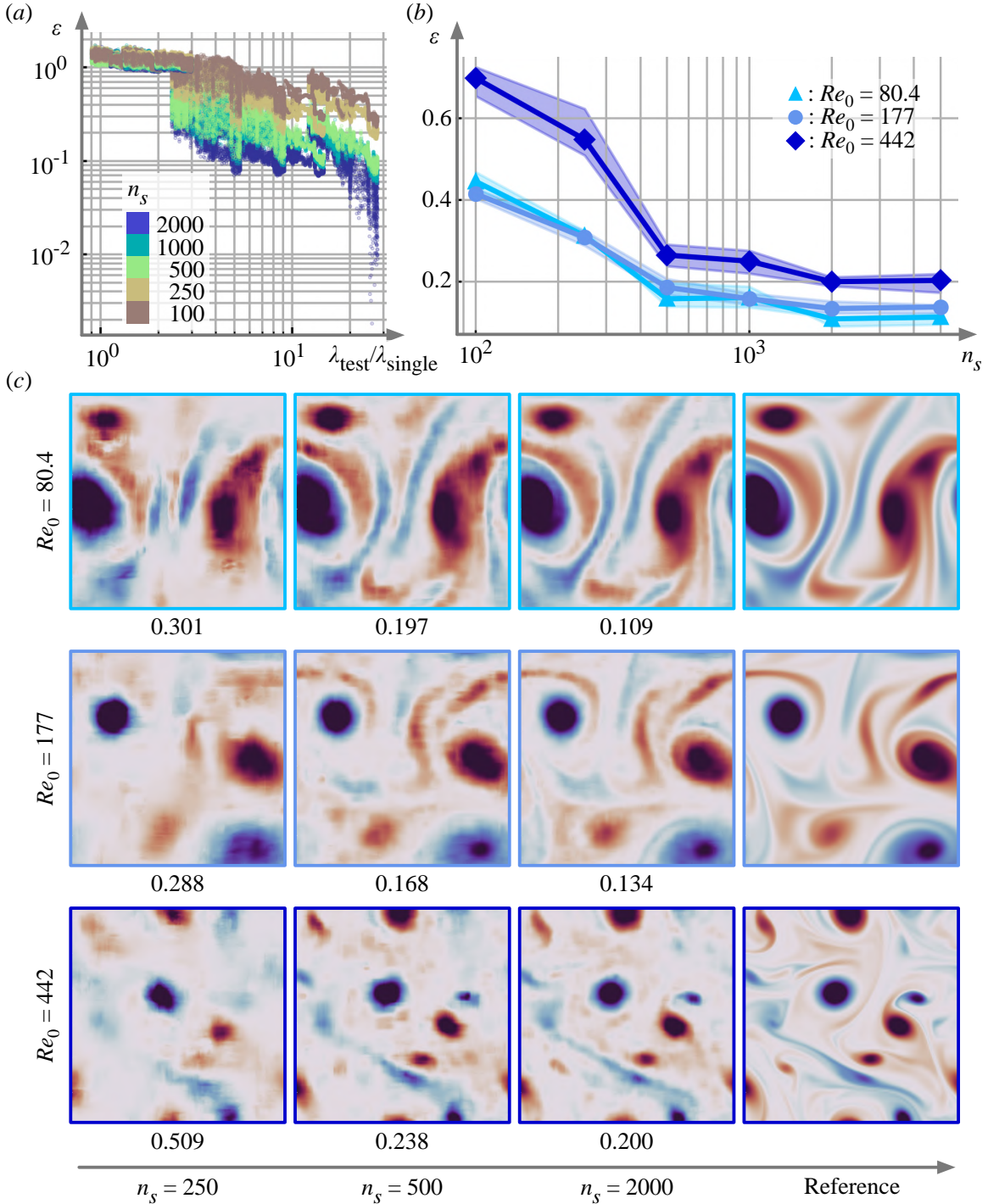


Figure 6: (a) The relationship between the reconstruction error ε and the ratio of the Taylor length scale between training and test snapshots $\lambda_{\text{test}}/\lambda_{\text{single}}$ across the number of training samples n_s . (b) Dependence of the reconstruction performance on the number of training samples n_s and (c) reconstructed vorticity fields for each test Reynolds number in using a single snapshot with $\lambda_{\text{single}} = 0.0425$ shown in figure 2. The value underneath each contour in figure (c) is the L_2 error norm.

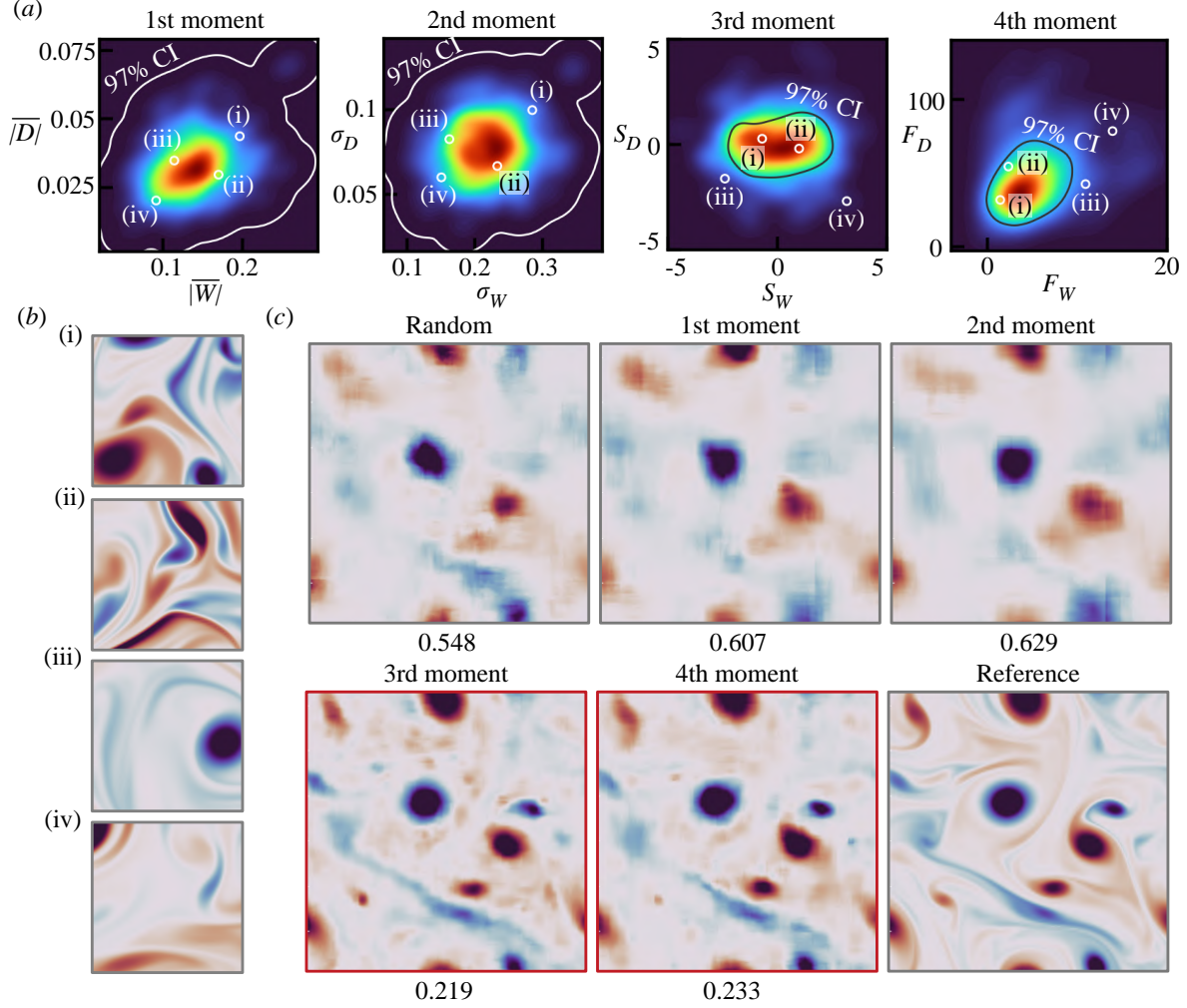


Figure 7: PDF-based sampling for single-snapshot training. (a) Two-dimensional PDF of first to fourth moments of rotation and strain tensors with $L_{\text{sub}} = 0.0625$. For each PDF map, 97% confidence interval is shown. (b) Example local tiles corresponding to (i-iv) on each PDF map. (c) Reconstruction with different data sampling with $n_s = 250$. The value underneath each contour reports the L_2 error norm.

4 Concluding remarks

This study discussed how we can efficiently extract physical insights from a very limited amount of turbulent flow data with machine learning. We considered machine-learning-based super-resolution reconstruction of two-dimensional decaying isotropic turbulence. The present convolutional network-based model trained with local flow subdomains collected from only a single snapshot provides accurate reconstruction for test data generated from different simulations. We further showed that training data for super-resolution analysis can be efficiently prepared from a single flow snapshot based on their statistical characteristics.

Although machine-learning-based analysis is often described as data-intensive, our findings indicate that it is possible to extract physical insights without over-relying on massive training data for studying turbulent flows. To capture scale invariant characteristics that are key for successful turbulent flow reconstruction with data-driven techniques, appropriate model architectures with physics embedding are important. The current results also suggest that redundancy of turbulent flows in not only space but also time can also be considered in sampling training data. By incorporating prior knowledge for developing a machine-learning model and collecting training data, we should be able to use smaller data sets to learn physics in a much smarter manner. We should stop being wasteful of turbulent flow data.

Acknowledgements

We thank the support from the US Air Force Office of Scientific Research (FA9550-21-1-0178) and the US Department of Defense Vannevar Bush Faculty Fellowship (N00014-22-1-2798).

Declaration of interests

The authors report no conflict of interest.

References

- [1] P. A. Davidson. *Turbulence: an introduction for scientists and engineers*. Oxford university press, 2015.
- [2] S. L. Brunton, B. R. Noack, and P. Koumoutsakos. Machine learning for fluid mechanics. *Annu. Rev. Fluid Mech.*, 52:477–508, 2020.
- [3] K. Duraisamy, G. Iaccarino, and H. Xiao. Turbulence modeling in the age of data. *Annu. Rev. Fluid. Mech.*, 51:357–377, 2019.
- [4] A. Racca, N. A. K. Doan, and L. Magri. Predicting turbulent dynamics with the convolutional autoencoder echo state network. *J. Fluid Mech.*, 975:A2, 2023.
- [5] K. Fukami, K. Fukagata, and K. Taira. Machine-learning-based spatio-temporal super resolution reconstruction of turbulent flows. *J. Fluid Mech.*, 909:A9, 2021.
- [6] L. Guastoni, A. Güemes, A. Ianiro, S. Discetti, P. Schlatter, H. Azizpour, and R. Vinuesa. Convolutional-network models to predict wall-bounded turbulence from wall quantities. *J. Fluid Mech.*, 928:A27, 2021.
- [7] T. Duriez, S. L. Brunton, and B. R. Noack. *Machine learning control – Taming nonlinear dynamics and turbulence*. Springer, 2017.
- [8] J. Park and H. Choi. Machine-learning-based feedback control for drag reduction in a turbulent channel flow. *J. Fluid Mech.*, 904:A24, 2020.
- [9] M. Raissi, P. Perdikaris, and G. E. Karniadakis. Physics-informed neural networks: A deep learning framework for solving forward and inverse problems involving nonlinear partial differential equations. *J. Comput. Phys.*, 378:686–707, 2019.
- [10] S. L. Brunton and J. N. Kutz. *Data-driven science and engineering: Machine learning, dynamical systems, and control*. Cambridge University Press, 2019.
- [11] S. Lee and D. You. Data-driven prediction of unsteady flow over a circular cylinder using deep learning. *J. Fluid Mech.*, 879:217–254, 2019.
- [12] K. Fukami, K. Fukagata, and K. Taira. Super-resolution analysis via machine learning: a survey for fluid flows. *Theor. Comput. Fluid Dyn.*, 37:421–444, 2023.
- [13] K. Fukami, K. Fukagata, and K. Taira. Super-resolution reconstruction of turbulent flows with machine learning. *J. Fluid Mech.*, 870:106–120, 2019.
- [14] Y. LeCun, L. Bottou, Y. Bengio, and P. Haffner. Gradient-based learning applied to document recognition. *Proc. IEEE*, 86(11):2278–2324, 1998.
- [15] K. Fukami, S. Goto, and K. Taira. Data-driven nonlinear turbulent flow scaling with Buckingham Pi variables. *J. Fluid Mech.*, 984:R4, 2024.
- [16] K. He, X. Zhang, S. Ren, and J. Sun. Deep residual learning for image recognition. In *Proceedings of the IEEE conference on computer vision and pattern recognition*, pages 770–778, 2016.
- [17] K. Taira, A. G. Nair, and S. L. Brunton. Network structure of two-dimensional decaying isotropic turbulence. *J. Fluid Mech.*, 795:R2, 2016.
- [18] G. I. Taylor. On the dissipation of eddies. *Meteorology, Oceanography and Turbulent Flow*, pages 96–101, 1918.
- [19] V. Anantharaman, J. Feldkamp, K. Fukami, and K. Taira. Image and video compression of fluid flow data. *Theor. Comput. Fluid Dyn.*, 37(1):61–82, 2023.
- [20] H. Kim, J. Kim, S. Won, and C. Lee. Unsupervised deep learning for super-resolution reconstruction of turbulence. *J. Fluid Mech.*, 910:A29, 2021.
- [21] M. Z. Yousif, M. Zhang, L. Yu, R. Vinuesa, and H. C. Lim. A transformer-based synthetic-inflow generator for spatially developing turbulent boundary layers. *J. Fluid Mech.*, 957:A6, 2023.